Inorganic Chemistry

Article

pubs.acs.org/IC

# Crystal Structure and Local Structure of $Mg_{2-x}Pr_xNi_4$ ($x$ = 0.6 and 1.0) Deuteride Using in Situ Neutron Total Scattering

K. Sakaki,*[,†] N. Terashita,[‡] H. Kim,[†] T. Proffen,[§] E. H. Majzoub,[#] S. Tsunokake,[‡] Y. Nakamura,[†] and E. Akiba[†,⊥]

[†]National Institute of Advanced Industrial Science and Technology, AIST Central-5, 1-1-1 Higashi, Tsukuba, Ibaraki, 305-0035, Japan

[‡]Japan Metals & Chemicals Co., Ltd., 232 Oguni, Nishiokitama, Yamagata 999-1351, Japan

[§]Lujan Neutron Scattering Center, Los Alamos National Laboratory, Los Alamos, New Mexico 87545, United States

[#]Center for Nanoscience, and Department of Physics and Astronomy, University of Missouri, St. Louis, Missouri 63121, United States

[⊥]Department of Mechanical Engineering, Faculty of Engineering and International Institute for Carbon-Neutral Energy Research (WPI-I2CNER), Kyushu University, 744 Motooka, Nishi-ku, Fukuoka 819-0395, Japan

**ABSTRACT:** We studied crystal structure and local structure of $Mg_{2-x}Pr_xNi_4$ ($x$ = 0.6 and 1.0) and their deuterides using in situ neutron total scattering and first-principles calculations. The total scattering data were analyzed using Rietveld refinement and pair distribution function analysis (PDF). The crystal structure of $Mg_{2-x}Pr_xNi_4$ before deuterium absorption was C15b in space group $F\bar{4}3m$. No difference between the crystal and local (PDF) structures was observed. The crystal structure of $Mg_{1.0}Pr_{1.0}Ni_4D_{\sim4}$ was found to be orthorhombic in space group $Pmn2_1$, with three deuterium occupation sites: $PrNi_3$ and two types of bipyramidal $Pr_2MgNi_2$ that have a plane of symmetry composed of $MgNi_2$. There is no significant difference between the crystal structure and the local structure of $Mg_{1.0}Pr_{1.0}Ni_4D_{\sim4}$. On the other hand, the average crystal structure of the Mg-rich $Mg_{1.4}Pr_{0.6}Ni_4D_{\sim3.6}$ was C15b with two deuterium occupation sites: $PrNi_3$ and $MgPrNi_2$ suggesting that the deuterium occupation shifts away from the $Pr_2MgNi_2$ bipyramid. First-principles relaxed structures also showed the shift of the hydrogen occupation site toward the Pr atom of the bipyramid, when induced by Mg substitution for the opposing Pr, resulting in hydrogen occupation in the $MgPrNi_2$ tetrahedral site. The PDF pattern of $Mg_{1.4}Pr_{0.6}Ni_4D_{\sim3.6}$ cannot be refined below 7.2 Å in atomic distances using the C15b structure which was obtained from Rietveld refinement but can be done using an orthorhombic structure. It suggests that $Mg_{1.4}Pr_{0.6}Ni_4D_{\sim3.6}$ was locally distorted to the orthorhombic.

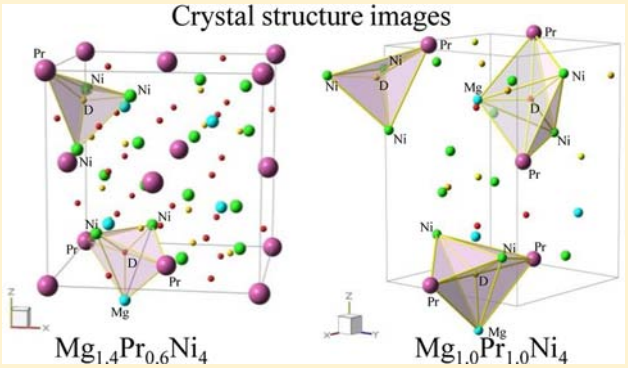


## 1. INTRODUCTION

Hydrogen storage materials have been extensively investigated for the nickel-hydride battery for many applications, including fuel cell vehicles. Various studies on the Mg-containing alloys such as hexagonal $PuNi_3$-type compounds (RE, Mg)$Ni_3$ (RE = rare earth)[1−4] and a C15b-type Laves phase $Mg_{1.0}Y_{1.0}Ni_4$[5] have been done to increase the gravimetric density and to tune the thermodynamic property. Chotard et al. found that $Mg_{1.0}La_{1.0}Ni_4$ absorbed hydrogen up to ∼1.0 H/M (H/M: ratio of the number of hydrogen and metal atoms) with two distinct plateaus on the pressure composition ($P-C$) isotherms,[6] although most of reported $Mg_{1.0}RE_{1.0}Ni_4$ absorbed only ∼0.7 H/M with one plateau.[7−12] We found that the dependence of Mg/RE ratio in $Mg_{2-x}RE_xNi_4$ on the hydrogenation properties and the crystal structures of the hydrides. The compounds with $x$ = 1.0 had two different hydride phases, an orthorhombic $Mg_{2-x}RE_xNi_4H_{\sim4}$ in space group $Pmn2_1$, and a cubic C15b $Mg_{2-x}RE_xNi_4H_{\sim6}$ (at high-hydrogen content), while those with $x$ < 1.0 (Mg-rich) had only cubic C15b $Mg_{2-x}RE_xNi_4H_{\sim3.6}$.[13−15] In addition, those compounds with $x$ > 1.0 transform to amorphous hydrides.[13] The dependence of the Mg/RE ratio on the crystal structure of hydrides likely originates from the different hydrogen occupation sites induced by the Mg/RE ratio.

Neutron total scattering is a powerful technique to solve crystal structures, especially for hydrogen storage materials because the deuterium occupation sites can be solved by Rietveld analysis of the Bragg peaks. Since the total scattering data includes not only the Bragg scattering but also the diffuse scattering, the total scattering experiment provides the information of both the crystal structure and the local structure. In general, a very large amount of the lattice defects and lattice strain are introduced upon hydrogenation in most hydrogen storage materials because of the large volume expansion.[16−26] These may lead the metal lattice to distort or atom positions to deviate from the average position determined by the Rietveld analysis. The atomic pair distribution function (PDF) is a local structural probing technique, utilizing scattering at large

**Received:** February 28, 2013
**Published:** May 31, 2013

   dx.doi.org/10.1021/ic400528u | Inorg. Chem. 2013, 52, 7010−7019

momentum transfer (large $2\theta$ scattering angle), that gives the probability of finding atom pairs separated by distance $r$.[27] The PDF analysis on neutron powder diffraction data reveals these local distortions and deviations, as well as deuterium occupation sites.

In this study, we investigated the crystal structure and the local structure of $Mg_{2-x}Pr_xNi_4$ ($x$ = 0.6 and 1.0) and their deuterides using neutron total scattering and first-principles calculations to understand the origin of the different crystal structures of the deuterides and to observe the local distortion upon deuterium absorption. The origin of different deuterium occupation sites and the local distortion will be discussed from the viewpoint of metal coordination changes with varying composition.

## 2. EXPERIMENTAL PROCEDURES

**2.1. Sample Preparation.**[13] The same alloy ingots that were investigated in ref 13 were used. Ingots of Mg, Pr, and Ni, each with purity higher than 99.9%, were used as the starting materials. $Mg_{1.0}Pr_{1.0}Ni_4$ and $Mg_{1.4}Pr_{0.6}Ni_4$ were prepared by high-frequency induction melting using an alumina crucible and were cast into a water-cooled board mold under a He atmosphere. The as-cast alloys were annealed at 1323 K for 10 h under an Ar atmosphere. The chemical analysis showed that the compositions of the annealed alloys were $Mg_{1.4}Pr_{0.6}Ni_{4.1}$ and $Mg_{1.0}Pr_{1.0}Ni_{4.0}$.

**2.2. Neutron Total Scattering Experiment.** The annealed alloys were crushed into powders and put into a stainless steel vessel. The vessel was evacuated by rotary pump at 423 K for more than 2 h. Deuterium absorption was carried out at room temperature at 5 MPa, and then deuterium desorption was carried out using a rotary pump at 423 K for more than 2 h. After several cycles of absorption and desorption of deuterium, the samples were taken out of the vessel and crushed into fine powders. These fine powders were loaded into a cylindrical high-pressure sample holder made of vanadium for in situ neutron total scattering. After evacuation for 2 h at 423 K, deuterium gas was introduced into sample holder up to 1 MPa to prepare the deuterides. Time-of-flight (TOF) neutron total scattering experiments were carried out on the NPDF instrument[28] at the Lujan Neutron Scattering Center at Los Alamos National Laboratory. Data sets for $Mg_{2-x}Pr_xNi_4$ and $Mg_{2-x}Pr_xNi_4D_{\sim y}$ ($x$ = 0.6 and 1.0) were collected for around 4 h at a temperature of 100 K to reduce the thermal vibration.

**2.3. Data Processing and Analysis for Neutron Total Scattering.** The signal from an empty container (a vanadium holder) was subtracted from the raw data, and various other corrections were made.[27] The PDF is obtained by a sine Fourier transformation of the powder diffraction data according to eq 1:

$$G(r) = \frac{2}{\pi}\int_{Q_{min}}^{Q_{max}} Q[S(Q) - 1]\sin(Qr)\,dQ, \quad (1)$$

where $Q$ is the magnitude of the momentum transfer and $S(Q)$ is the total scattering structure function.[27] Because of the unfavorable signal-to-noise ratio at the high-$Q$ regions, $Q[S(Q)\text{-}1]$ was truncated at $Q_{max}$ = 35 Å$^{-1}$ for neutron data before the transformation. Data processing program PDFgetN[29] was used for obtaining neutron PDFs. Real space modeling was carried out using the PDFgui program.[30] The PDF is simply a bond length distribution, and therefore the PDF of a given structure can be calculated using the following equation:

$$G(r) = \frac{1}{r}\sum_i\sum_j\left[\frac{b_i b_j}{\langle b\rangle^2}\delta(r - r_{ij})\right] - 4\pi r\rho_0 \quad (2)$$

where $b_i$ is the scattering power of atom $i$ (neutron scattering lengths), $<b>$ is the average scattering power of the sample, $r_{ij}$ is the distance between atoms $i$ and $j$, and $\rho_0$ is the number density.[31] The sums go over all the atoms in the model crystal. It is worth noting that the intensity of a PDF peak located at $r$ is proportional to the number of atom pairs separated by distance $r$ and the scattering powers of the contributing atoms.

Structural refinement in reciprocal space was carried out by Rietveld analysis using the EXPGUI-GSAS program.[32,33] Four patterns with different $d$ space obtained from the different detectors were analyzed simultaneously.

**2.4. Computational Method.** First-principles calculations were performed to understand the effect of substitution of Mg and Pr atoms on the hydrogen occupation site energies using the Vienna *ab initio* simulation package (VASP) package.[34,35] The generalized gradient approximation (GGA) proposed by Perdew et al.[36] was used for the exchange-correlation functional. We used the VASP Pr potential where f-electrons are kept frozen in the core. This is a standard model for the treatment of localized f electrons. The potentials based upon the all-electron projector augmented wave (PAW) method were used.[37,38] The structure relaxations were performed until the maximum force dropped below 0.001 eV/Å, with a self-consistent field (SCF) convergence criterion of $10^{-7}$ eV. The plane wave cutoff energy was chosen to be 425 eV. The k-point spacing was chosen to be 0.15 Å$^{-1}$.

Three structure models with compositions $Mg_4Pr_4Ni_{16}H_1$, $Mg_5Pr_3Ni_{16}H_1$, and $Mg_3Pr_5Ni_{16}H_1$ were created. (1) The $Mg_4Pr_4Ni_{16}$ structure model with C15b structure was initially created with a hydrogen atom placed at (0.25, 0.25, 0). This is the center of a $Pr_2MgNi_2$ bipyramidal interstitial site and is on the $MgNi_2$ symmetry plane for the bipyramid. (2) The Pr atom at (0,0,0), an end cap of the bipyramid, was replaced by Mg to create the $Mg_5Pr_3Ni_{16}H_1$ structure model, breaking the mirror symmetry of the bipyramid. (3) To create the $Mg_3Pr_5Ni_{16}H_1$ structure model, the Mg atom that is the nearest neighbor of the hydrogen atom was replaced by Pr (the symmetry plane of the bipyramid is now $PrNi_2$). Two types of structure relaxation were carried out. One was fully structure relaxation in which the atomic positions, cell volume, and cell shape were all allowed to change. In the second, to retain the cubic structure, the cell volume only was initially optimized and then the atomic positions were optimized, and these processes were repeated more than three times.

## 3. RESULTS

**3.1. Crystal Structure and Local Structure of $Mg_{1.0}Pr_{1.0}Ni_4$ and $Mg_{1.4}Pr_{0.6}Ni_4$ Alloys.** Figure 1a,b shows the results of Rietveld refinement for the neutron diffraction patterns of $Mg_{1.0}Pr_{1.0}Ni_4$ and $Mg_{1.4}Pr_{0.6}Ni_4$ measured at 100 K. The crystal structure was a C15b with space group $F\bar{4}3m$. The refined lattice constants of $Mg_{1.0}Pr_{1.0}Ni_4$ and $Mg_{1.4}Pr_{0.6}Ni_4$ were 7.0827 and 7.0068 Å, respectively. These agree with our previous XRD results.[13,15] Table 1 shows the refined atomic positions of $Mg_{1.0}Pr_{1.0}Ni_4$ and $Mg_{1.4}Pr_{0.6}Ni_4$. The obtained atomic displacement parameters, $U$, were reasonable values.

Figure 1c,d shows the result of local structure analysis for the pair distribution function of $Mg_{1.0}Pr_{1.0}Ni_4$ and $Mg_{1.4}Pr_{0.6}Ni_4$. The structure models obtained from the Rietveld refinement were used for the local structure analysis as the initial structure model. The simulated $G(r)$ fits the measured data very well. The refined atomic positions of $Mg_{1.0}Pr_{1.0}Ni_4$ and $Mg_{1.4}Pr_{0.6}Ni_4$ using PDF analysis is shown in Table 2. These results indicate that no significant difference between the average structure and the local structure was observed for the alloys.

**3.2. Crystal Structure and Local Structure of $Mg_{1.0}Pr_{1.0}Ni_4D_{\sim 4}$.** Before the neutron experiment, it was confirmed that the isotope effect on the crystal structure of metal lattice and the hydrogenation properties such as hydrogen content and equilibrium pressure were not observed in $Mg_{1.0}Pr_{1.0}Ni_4$. Figure 2a shows the result of Rietveld refinement for the neutron diffraction pattern of $Mg_{1.0}Pr_{1.0}Ni_4D_{\sim 4}$ measured at 100 K. The crystal structure was an orthorhombic structure with space group $Pmn2_1$ that was the same as the crystal structure of $Mg_{1.0}La_{1.0}Ni_4D_{3.7}$ and $Mg_{1.0}Nd_{1.0}Ni_4D_{3.6}$.[6,8] The lattice constants of $Mg_{1.0}Pr_{1.0}Ni_4D_{\sim 4}$ were $a$ = 5.0829 (1) Å, $b$ = 5.4729 (1) Å, and $c$ = 7.3838 (2) Å. The volume


dx.doi.org/10.1021/ic400528u | Inorg. Chem. 2013, 52, 7010−7019

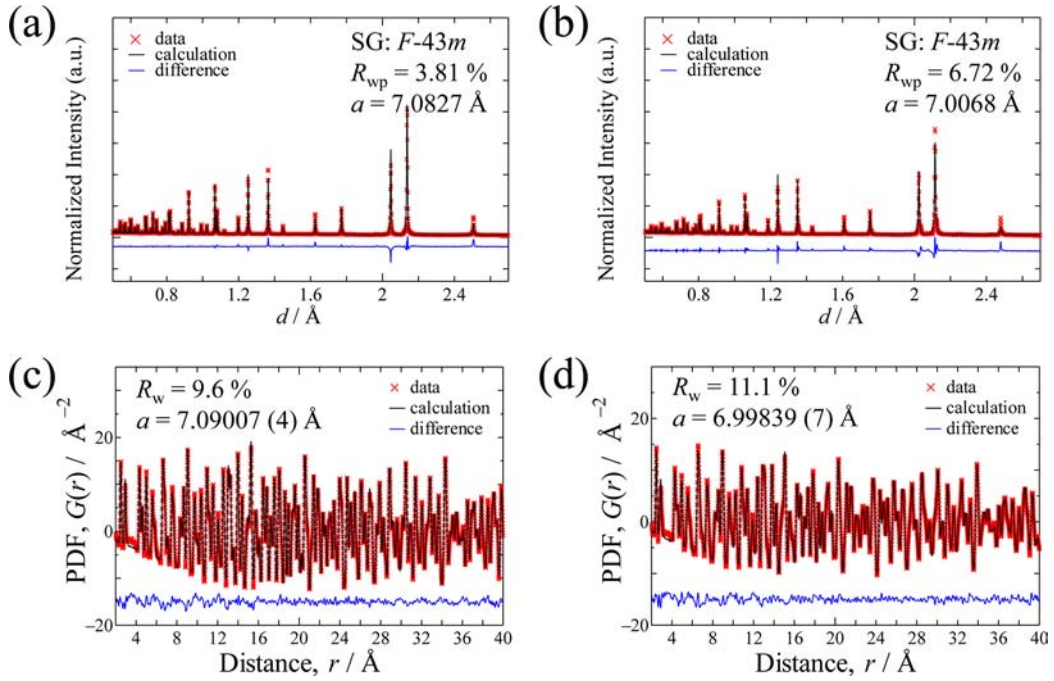


**Figure 1.** Results of Rietveld and PDF analyses of neutron total scattering data measured at 100 K; (a) and (b) Rietveld analyses for $Mg_{1.0}Pr_{1.0}Ni_4$ and $Mg_{1.4}Pr_{0.6}Ni_4$, (c) and (d) PDF analyses for $Mg_{1.0}Pr_{1.0}Ni_4$ and $Mg_{1.4}Pr_{0.6}Ni_4$.

**Table 1. Refined Atomic Coordination of $Mg_{1.0}Pr_{1.0}Ni_4$ (a) and $Mg_{1.4}Pr_{0.6}Ni_4$ (b) by Rietveld Refinement**

| (a) $Mg_{1.0}Pr_{1.0}Ni_4$: space group $F\bar{4}3m$, $a$ = 7.0827 Å $R_w$ = 3.81% | | | | | | |
|---|---|---|---|---|---|---|
| atom | Wyckoff position | $x$ | $y$ | $z$ | $U$/Å$^2$ | occupancy |
| Pr | 4*a* | 0 | 0 | 0 | 0.0051 (7) | 1 |
| Mg | 4*c* | 0.25 | 0.25 | 0.25 | 0.0075 (6) | 1 |
| Ni | 16*e* | 0.62359 (6) | 0.62359 (6) | 0.62359 (6) | 0.00534 (5) | 1 |
| (b) $Mg_{1.4}Pr_{0.6}Ni_4$: space group $F\bar{4}3m$, $a$ = 7.0068 Å $R_w$ = 6.72% | | | | | | |
| atom | Wyckoff position | $x$ | $y$ | $z$ | $U$/Å$^2$ | occupancy |
| Pr | 4*a* | 0 | 0 | 0 | 0.007 (1) | 0.6 |
| Mg | 4*a* | 0 | 0 | 0 | =Pr | 0.4 |
| Mg | 4*c* | 0.25 | 0.25 | 0.25 | 0.013 (1) | 1 |
| Ni | 16*e* | 0.6264 (3) | 0.6264 (3) | 0.6264 (3) | 0.0074 (1) | 1 |

**Table 2. Refined Atomic Coordination of $Mg_{1.0}Pr_{1.0}Ni_4$ (a) and $Mg_{1.4}Pr_{0.6}Ni_4$ (b) by PDF Refinement**

| (a) $Mg_{1.0}Pr_{1.0}Ni_4$: space group $F\bar{4}3m$, $a$ = 7.09007 (4) Å, $R_w$ = 9.6% | | | | | | |
|---|---|---|---|---|---|---|
| atom | Wyckoff position | $x$ | $y$ | $z$ | $U$/Å$^2$ | occupancy |
| Pr | 4*a* | 0 | 0 | 0 | 0.0036 (3) | |
| Mg | 4*c* | 0.25 | 0.25 | 0.25 | 0.0035 (3) | 1 |
| Ni | 16*e* | 0.62334 (4) | 0.62334 (4) | 0.62334 (4) | 0.00272 (2) | 1 |
| (b) $Mg_{1.4}Pr_{0.6}Ni_4$: space group $F\bar{4}3m$, $a$ = 6.99839 (7) Å $R_w$ = 11.1% | | | | | | |
| atom | Wyckoff position | $x$ | $y$ | $z$ | $U$/Å$^2$ | occupancy |
| Pr | 4*a* | 0 | 0 | 0 | 0.007 (5) | 0.6 |
| Mg | 4*a* | 0 | 0 | 0 | =Pr | 0.4 |
| Mg | 4*c* | 0.25 | 0.25 | 0.25 | 0.007 (5) | 1 |
| Ni | 16*e* | 0.625 (2) | 0.625 (2) | 0.625 (2) | 0.00443 (3) | 1 |

expansion was 15.6%, which is consistent with those for $Mg_{1.0}Pr_{1.0}Ni_4H_{\sim4}$ (15.4%),[15] $Mg_{1.0}La_{1.0}Ni_4D_{3.7}$ (14.5%),[6] and $Mg_{1.0}Nd_{1.0}Ni_4D_{3.6}$ (14.6%).[8] The obtained atomic coordination is shown in Table 3a, and these values were consistent with the values reported for $Mg_{1.0}Nd_{1.0}Ni_4D_{\sim3.6}$[8] and $Mg_{1.0}La_{1.0}Ni_4D_{\sim3.7}$[6] and the optimized atomic coordination for $Mg_{1.0}RE_{1.0}Ni_4H_4$ using *ab initio* calculations.[14] There were three deuterium occupation sites. Two of them were the $Pr_2MgNi_2$ triangular bipyramid (4*b*, 2*a*), and the other was the $PrNi_3$ tetrahedron (2*a*). The occupancy of these sites was refined, but the obtained values were close to 1 and the $R_{wp}$ value did not change. Therefore, they were fixed at the value of 1. The number of deuterium atoms in the structure model used for the refinement was similar to the experimental value evaluated from the $P-C$ isotherm. In addition the shortest distance between two deuterium atoms was 2.502 Å, which is larger than Westlake's


dx.doi.org/10.1021/ic400528u | *Inorg. Chem.* 2013, 52, 7010−7019

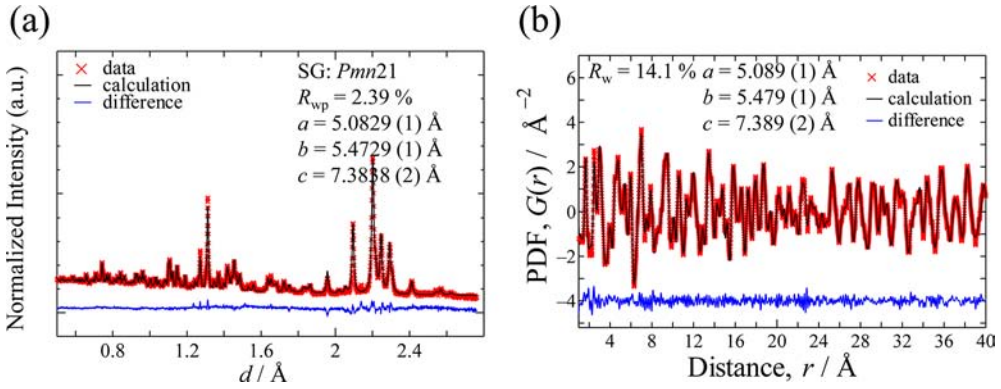


**Figure 2.** Result of Rietveld (a) and PDF analyses (b) for $Mg_{1.0}Pr_{1.0}Ni_4D_{\sim4}$ measured at 100 K.

**Table 3. Refined Atomic Coordination of $Mg_{1.0}Pr_{1.0}Ni_4D_{\sim4}$; (a) Rietveld Analysis and (b) PDF Analysis**

| (a) $Mg_{1.0}Pr_{1.0}Ni_4D_{\sim4}$: space group *Pmn*21, $a$ = 5.0829 (1) Å, $b$ = 5.4729 (1) Å, $c$ = 7.3838 (2) Å, $R_w$ = 2.39% | | | | | | |
|---|---|---|---|---|---|---|
| atom | Wyckoff position | $x$ | $y$ | $z$ | $U$/Å$^2$ | occupancy |
| Pr | 2*a* | 0 | 0.3000 (6) | 0.0045 (4) | 0.0096 (6) | 1 |
| Mg | 2*a* | 0 | 0.8076 (6) | 0.2264 (4) | 0.0208 (6) | 1 |
| Ni | 2*a* | 0 | 0.4476 (2) | 0.6231 (1) | 0.0073 (2) | 1 |
| Ni | 2*a* | 0 | 0.9914 (2) | 0.6071 (2) | 0.0087 (2) | 1 |
| Ni | 4*b* | 0.7567 (2) | 0.2294 (2) | 0.3832 (1) | 0.0081 (1) | 1 |
| D | 4*b* | 0.7462 (3) | 0.5096 (3) | 0.759 (2) | 0.0195 (3) | 1 |
| D | 2*a* | 0 | 0.7204 (5) | 0.5103 (3) | 0.0184 (5) | 1 |
| D | 2*a* | 0 | 0.9414 (4) | 0.8278 (2) | 0.0175 (5) | 1 |
| (b) $Mg_{1.0}Pr_{1.0}Ni_4D_{\sim4}$: space group *Pmn*21, $a$ = 5.089 (1) Å, $b$ = 5.479 (1) Å, $c$ = 7.389 (2) Å, $R_w$ = 14.1% | | | | | | |
| atom | Wyckoff position | $x$ | $y$ | $z$ | $U$/Å$^2$ | occupancy |
| Pr | 2*a* | 0 | 0.303 (3) | 0.005 (3) | 0.005 (1) | 1 |
| Mg | 2*a* | 0 | 0.814 (3) | 0.229 (3) | 0.007 (2) | 1 |
| Ni | 2*a* | 0 | 0.448 (2) | 0.626 (1) | 0.0058 (9) | 1 |
| Ni | 2*a* | 0 | 0.992 (1) | 0.611 (1) | 0.0051 (8) | 1 |
| Ni | 4*b* | 0.757 (1) | 0.229 (1) | 0.384 (1) | 0.0055 (5) | 1 |
| D | 4*b* | 0.749 (3) | 0.507 (2) | 0.762 (1) | 0.012 (1) | 1 |
| D | 2*a* | 0 | 0.732 (4) | 0.511 (3) | 0.015 (2) | 1 |
| D | 2*a* | 0 | 0.939 (4) | 0.826 (3) | 0.014 (2) | 1 |

empirical criteria of 2.1 Å.[39] It indicates that the repulsive interactions are unlikely to interrupt the deuterium occupation. Therefore, a full occupation structure model is reasonable.

Figure 2b shows the fitting result of the PDF of $Mg_{1.0}Pr_{1.0}Ni_4D_{\sim4}$ for local structure analysis. The structure model obtained from the Rietveld refinement was used as an initial model. The occupancy of deuterium sites was refined, but the obtained values were close to and slightly above 1. Therefore, deuterium occupancy was also fixed at a value of 1. The refined atomic positions from a PDF analysis are shown in Table 3b. The result of the local structure analysis is in good agreement with the Rietveld analysis. No significant difference between the average structure and the local structure was observed in $Mg_{1.0}Pr_{1.0}Ni_4D_{\sim4}$.

**3.3. Crystal Structure and Local Structure of $Mg_{1.4}Pr_{0.6}Ni_4D_{\sim3.6}$.** Before the neutron experiment, it was confirmed that the isotope effect on the crystal structure of metal lattice and the hydrogenation properties were not observed in $Mg_{1.4}Pr_{0.6}Ni_4$. Figure 3a shows the result of Rietveld refinement for the neutron diffraction pattern of $Mg_{1.4}Pr_{0.6}Ni_4D_{\sim3.6}$. The crystal structure was a C15b with space group $F\bar{4}3m$, which is the same as the alloy phase. The lattice constant of $Mg_{1.4}Pr_{0.6}Ni_4D_{\sim3.6}$ was $a$ = 7.3409 (1) Å. The volume expansion was 15.0%, which is close to that for $Mg_{1.4}Pr_{0.6}Ni_4H_{\sim3.6}$ (13.4%), $Mg_{1.4}Sm_{0.6}Ni_4H_{\sim3.6}$ (15.1%), and $Mg_{1.4}Gd_{0.6}Ni_4H_{\sim3.6}$ (14.1%).[14,15] The expansion was also close to that for $Mg_{1.0}Pr_{1.0}Ni_4D_{\sim4}$ even though the crystal structures were different. The obtained atomic coordinates are shown in Table 4. There were two deuterium occupation sites, $PrNi_3$ tetrahedron (16*e*) and $PrMgNi_2$ tetrahedron (48*h*) as shown in Figure 3b. The deuterium occupation sites were different from those in $Mg_{1.0}Pr_{1.0}Ni_4D_{\sim4}$. The deuterium atom in the $PrMgNi_2$ tetrahedron was located near the $MgNi_2$ plane, but not in the plane. It suggests that the deuterium occupation site shifted from the center of the $Pr_2MgNi_2$ triangular bipyramid (24*g*) toward the center of the $PrMgNi_2$ tetrahedron. The occupancy of deuterium at these sites was small, as shown in Table 4, in accordance with the larger multiplicity of the Wyckoff position. The number of deuterium atoms in the refined structure model was 14.24, close to that evaluated from $P-C$ isotherms (14.4). The obtained atomic displacement parameters $U$ were relatively larger than usual values which were obtained in $Mg_{2-x}Pr_xNi_4$ and $Mg_{1.0}Pr_{1.0}Ni_4D_{\sim4}$. Another structure model in which the deuterium atoms occupy the high-symmetry center of $Pr_2MgNi2$ triangular bipyramid (24*g*) instead of $PrMgNi_2$ tetrahedron (48*h*) was also applied. The number of deuterium atoms in the unit cell did not change, but the atomic displacement parameter of this deuterium site became larger and $R_{wp}$ value became worse. Since almost half of Pr atoms were replaced by Mg atoms in $Mg_{1.4}Pr_{0.6}Ni_4D_{\sim3.6}$, many


dx.doi.org/10.1021/ic400528u | Inorg. Chem. 2013, 52, 7010−7019

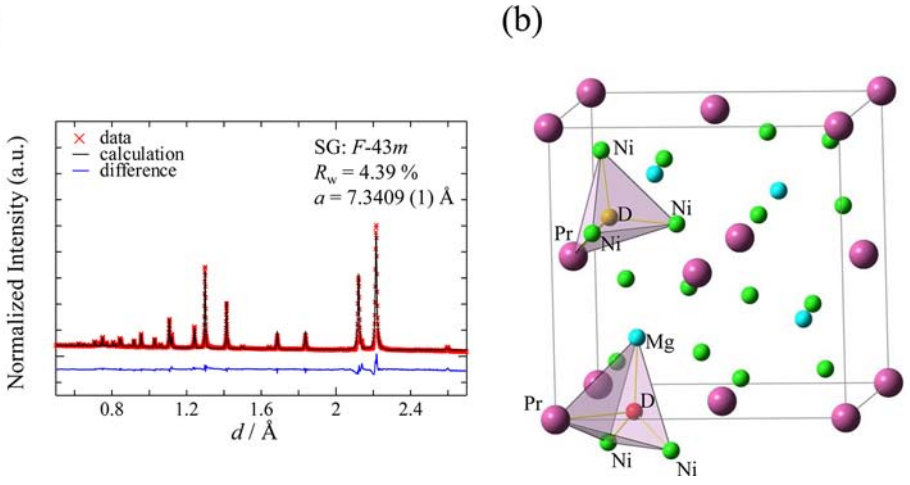


**Figure 3.** (a, b) Result of Rietveld analysis for $Mg_{1.4}Pr_{0.6}Ni_4D_{\sim 3.6}$ measured at 100 K.

**Table 4. Refined Atomic Coordination of $Mg_{1.4}Pr_{0.6}Ni_4D_{\sim 3.6}$; (a) Rietveld Analysis and (b) PDF Analysis to 7.2 Å (c) PDF Analysis from 7.2 to 40 Å**

| (a) $Mg_{1.4}Pr_{0.6}Ni_4D_{\sim 3.6}$: space group *F*-43*m*, $a$ = 7.3409 (1) Å, $R_w$ = 4.39% | | | | | | |
|---|---|---|---|---|---|---|
| atom | Wyckoff position | $x$ | $y$ | $z$ | $U$/Å$^2$ | occupancy |
| Pr | 4*a* | 0 | 0 | 0 | 0.029 (1) | 0.6 |
| Mg | 4*a* | 0 | 0 | 0 | 0.16 (1) | 0.4 |
| Mg | 4*c* | 0.25 | 0.25 | 0.25 | 0.085 (2) | 1 |
| Ni | 16*e* | 0.6231 (1) | 0.6231 (1) | 0.6231 (1) | 0.0256 (2) | 1 |
| D | 16*e* | 0.8493 (2) | 0.8493 (2) | 0.8493 (2) | 0.018 (1) | 0.290 (6) |
| D | 48*h* | 0.7363 (5) | 0.7363 (5) | 0.9979 (3) | 0.0196 (7) | 0.200 (2) |
| (b) $Mg_{1.4}Pr_{0.6}Ni_4D_{\sim 3.6}$: space group *Pmn*21, $a$ = 5.104 (8) Å, $b$ = 5.33 (1) Å, $c$ = 7.35 (1) Å, $R_w$ = 12.6% | | | | | | |
| atom | Wyckoff position | $x$ | $y$ | $z$ | $U$/Å$^2$ | occupancy |
| Pr | 2*a* | 0 | 0.347 (5) | 0.018 (4) | 0.003 (3) | 0.6 |
| Mg | 2*a* | =Pr | =Pr | =Pr | =Pr | 0.4 |
| Mg | 2*a* | 0 | 0.695 (7) | 0.256 (5) | 0.013 (5) | 1 |
| Ni | 2*a* | 0 | 0.507 (2) | 0.593 (1) | 0.003 (1) | 1 |
| Ni | 2*a* | 0 | 0.028 (4) | 0.648 (3) | 0.016 (3) | 1 |
| Ni | 4*b* | 0.751 (2) | 0.233 (2) | 0.378 (2) | 0.0068 (9) | 1 |
| D | 4*b* | 0.763 (3) | 0.508 (2) | 0.755 (2) | 0.009 (1) | 1 |
| D | 2*a* | 0 | 0.716 (5) | 0.502 (3) | 0.008 (3) | 1 |
| D | 2*a* | 0 | 0.933 (2) | 0.864 (2) | 0.007 (2) | 1 |
| (c) $Mg_{1.4}Pr_{0.6}Ni_4D_{\sim 3.6}$: space group $F\bar{4}3m$, $a$ = 7.3484 (4) Å, $R_w$ = 13.1% | | | | | | |
| atom | Wyckoff position | $x$ | $y$ | $z$ | $U$/Å$^2$ | occupancy |
| Pr | 4*a* | 0 | 0 | 0 | 0.038 (6) | 0.6 |
| Mg | 4*a* | 0 | 0 | 0 | =Pr | 0.4 |
| Mg | 4*c* | 0.25 | 0.25 | 0.25 | 0.10 (1) | 1 |
| Ni | 16*e* | 0.6237 (8) | 0.6237 (8) | 0.6237 (8) | 0.0234 (5) | 1 |
| D | 16*e* | 0.848 (1) | 0.848 (1) | 0.848 (1) | 0.022 (4) | 0.2898 |
| D | 48*h* | 0.75 (1) | 0.75 (1) | 0.992 (1) | 0.024 (1) | 0.1999 |

$Pr_2MgNi_2$ bipyramids become $PrMg_2Ni_2$, which is asymmetric to the $MgNi_2$ plane. The refinements indicate that it is favorable to shift the deuterium position in this asymmetric $PrMg_2Ni_2$ to either the $PrMgNi_2$ tetrahedron or $Mg_2Ni_2$ tetrahedron. Therefore, the structure model where deuterium atoms occupy the 48*h* site is more reasonable than that for the 24*g* site.

Figure 4 shows the result of local structure analysis for the pair distribution function of $Mg_{1.4}Pr_{0.6}Ni_4D_{\sim 3.6}$. The structure models obtained from the Rietveld refinement (C15b structure) were used for the local structure analysis. When analysis was performed in the $r$ range from 7.2 Å to 40 Å, the refinement agreements are rather good with $R_{wp}$ values less than 13.1%. The atomic coordination was consistent with that obtained from Rietveld refinement as shown in Table 4. However, when the refinement region was expanded to 1 Å $\leq r \leq$ 40 Å, the simulated $G(r)$ curve using this structure model did not fit well in the $r$ range from 1 Å to 4 Å as shown in Figure 4a. This suggests that the local structure of this hydride was different from the average structure in C15b, especially below 7.2 Å in atomic distances. The first peak of the measured $G(r)$ curve was around 1.64 Å but that of the simulated $G(r)$ one was around 1.56 Å. The first peak of the $G(r)$ curve mainly corresponds to the Ni−D bonding. It suggests that the Ni and/or D positions have deviated from the average position.


dx.doi.org/10.1021/ic400528u | *Inorg. Chem.* 2013, 52, 7010−7019

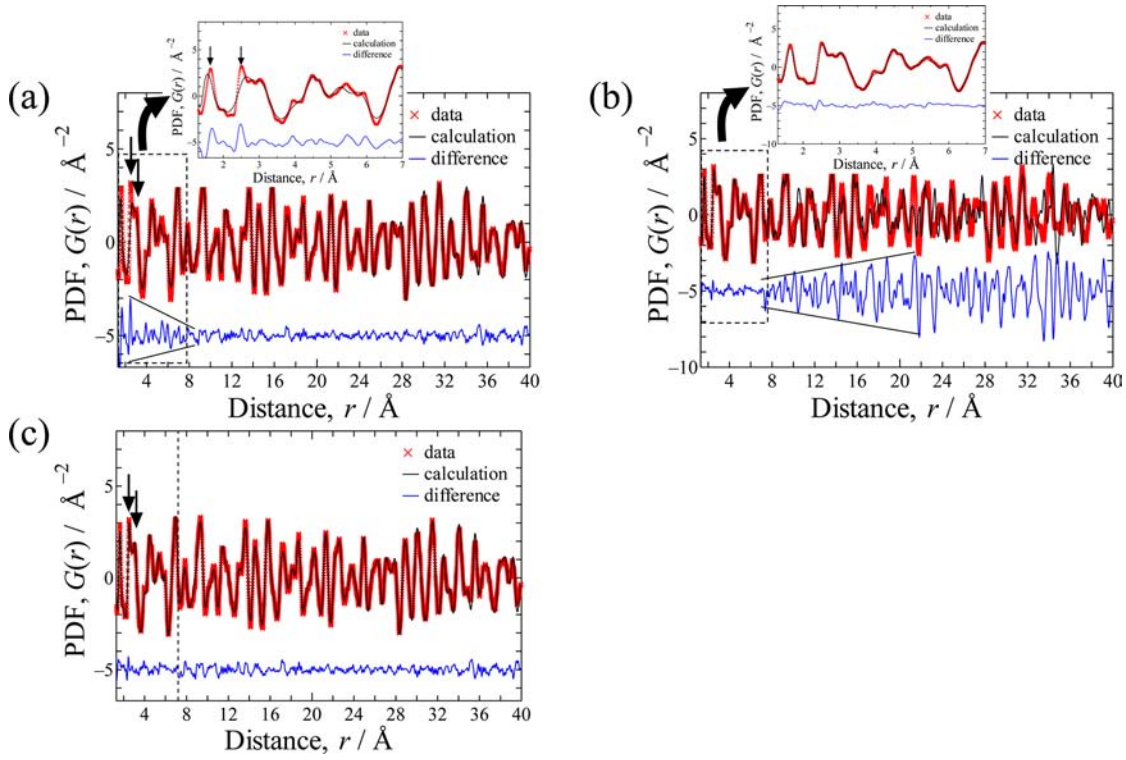


**Figure 4.** Result of PDF analysis for $Mg_{1.4}Pr_{0.6}Ni_4D_{\sim 3.6}$ measured at 100 K. (a) C15b structure model, (b) orthorhombic structure model, and (c) orthorhombic + C15b structure model.

Below 7.2 Å in atomic distances, we applied the structure model with an orthorhombic structure with $Pmn2_1$, which is the same as the crystal structure of $Mg_{1.0}Pr_{1.0}Ni_4D_{\sim 4}$ instead of a C15b structure. By changing the structure model, the bond length between Ni-D increased to 1.63 Å, which is close to the position of the first peak for the measured $G(r)$ curve, 1.64 Å. As shown in Figure 4b, this structure model worked well below 7.2 Å, and the fitting was dramatically improved. However, the difference between the simulated $G(r)$ curve and measured data became larger with the increase of $r$ above 7.2 Å in atomic distances. These data suggest that $Mg_{1.4}Pr_{0.6}Ni_4D_{\sim 3.6}$ was distorted orthorhombic $Pmn2_1$ in local structure, although the average structure is still C15b. The domain size showing the orthorhombic structure was around 7.2 Å in atomic distances, which was close to the lattice constant of a C15b $Mg_{1.4}Pr_{0.6}Ni_4D_{\sim 3.6}$ as shown in Figure 4c. This means that the structure within each domain with 7.2 Å in size was orthorhombic and these domains randomly distributed to keep the crystal structure the C15b structure in average.

**3.4. Effect of the Mr/Pr Ratio on the Hydrogen Occupation Site.** In order to investigate the effect of the Mg/Pr ratio on the hydrogen occupation site, structure relaxations for $Mg_4Pr_4Ni_{16}H_1$, $Mg_5Pr_3Ni_{16}H_1$, and $Mg_3Pr_5Ni_{16}H_1$ were carried out using first-principles calculations. The optimized lattice constants and atomic coordination of $MgPr_2Ni_2$ triangular bipyramid that was obtained by the volume optimization and the atomic optimization independently are shown in Table 5. Since the lattice constants of each alloy phase were 7.126693 Å for $Mg_4Pr_4Ni_{16}$, 7.058227 Å for $Mg_5Pr_3Ni_{16}$, and 7.186915 Å for $Mg_3Pr_5Ni_{16}$, respectively, the volume expansions were around 1%. In $Mg_4Pr_4Ni_{16}H_1$, the $Pr_2MgNi_2$ triangular bipyramid site was found to retain the symmetry of the Mg-Ni-Ni plane; the hydrogen atom remained on the Mg-Ni-Ni plane of $Pr_2MgNi_2$ triangular bipyramid suggesting that the hydrogen atom was on the 24$g$ site as shown in Figure 5a. The distance between Pr and H atoms was 2.492 Å. When the Mg atom in $Pr_2MgNi_2$ triangular bipyramid was replaced by a Pr atom as shown in Figure 5b, the hydrogen atom still sit on the Mg-Ni-Ni plane of $Pr_2MgNi_2$ triangular bipyramid, but the hydrogen atom shifted away from the substituted Pr atom because the Pr atom (1.83 Å) is larger than the Mg atom (1.6 Å). This triangular bipyramid is still symmetrical about the Mg-Ni-Ni plane. The distance between Pr and H atoms was 2.595 Å. On the other hand, when one of Pr atoms in $Pr_2MgNi_2$ was replaced by Mg as shown in Figure 5c, the triangular bipyramid became asymmetric about the Mg-Ni-Ni plane and then the hydrogen atom did not sit on the Mg-Ni-Ni plane. The distances for H-Pr and H-substituted Mg were 2.414 Å and 2.543 Å, respectively. These results indicated that the hydrogen occupation site was influenced by the substitution of Mg into Pr and hydrogen atoms prefer to occupy the $PrMgNi_2$ tetrahedron rather than the $Mg_2Ni_2$ tetrahedron. A similar result was obtained when full structure relaxation was carried out even though the shape of unit cell was slightly distorted from a cubic.

## 4. DISCUSSION

**4.1. Deuterium Coordination in $Mg_{1.4}Pr_{0.6}Ni_4D_{\sim 3.6}$ in Average and Local.** As described above, $Mg_{1.4}Pr_{0.6}Ni_4D_{\sim 3.6}$ showed a distortion from cubic to orthorhombic in the local order. We will discuss the deuterium coordination in $Mg_{1.4}Pr_{0.6}Ni_4D_{\sim 3.6}$ and then the difference between the average and local structures.

The deuterium occupation sites in $Mg_{1.4}Pr_{0.6}Ni_4D_{\sim 3.6}$ were $PrNi_3$ tetrahedron (16$e$) and $PrMgNi_2$ tetrahedron (48$h$) in the average structure. To simplify the model, the deuterium occupation site is assumed to be the 24$g$ site at (0.75, 0.75, 0.9979),


dx.doi.org/10.1021/ic400528u | Inorg. Chem. 2013, 52, 7010−7019

**Table 5. Atomic Coordination of $Mg_{2-x}Pr_xNi_{16}H_1$; (a) $Mg_4Pr_4Ni_{16}H_1$, (b) $Mg_3Pr_5Ni_{16}H_1$, and (c) $Mg_5Pr_3Ni_{16}H_1$**

| (a) $Mg_4Pr_4Ni_{16}H_1$, $a$ = 7.14192162245 Å | | | |
|---|---|---|---|
| atom | $x$ | $y$ | $z$ |
| H1 | 0.25 | 0.25 | 0.988403323 |
| Mg1 | 0.25 | 0.25 | 0.271719226 |
| Mg2 | 0.25 | 0.75 | 0.749343429 |
| Mg3 | 0.75 | 0.25 | 0.749343429 |
| Mg4 | 0.75 | 0.75 | 0.245169177 |
| Ni1 | 0.12379806 | 0.12379806 | 0.621071906 |
| Ni2 | 0.113784128 | 0.386215872 | 0.874762779 |
| Ni3 | 0.1191306 | 0.628581326 | 0.124467342 |
| Ni4 | 0.125239649 | 0.878389607 | 0.37650867 |
| Ni5 | 0.386215872 | 0.113784128 | 0.874762779 |
| Ni6 | 0.3808694 | 0.871418674 | 0.124467342 |
| Ni7 | 0.628581326 | 0.1191306 | 0.124467342 |
| Ni8 | 0.626132034 | 0.873867966 | 0.875358958 |
| Ni9 | 0.878389607 | 0.125239649 | 0.37650867 |
| Ni10 | 0.871418674 | 0.3808694 | 0.124467342 |
| Ni11 | 0.873867966 | 0.626132034 | 0.875358958 |
| Ni12 | 0.878402817 | 0.878402817 | 0.623712443 |
| Ni13 | 0.37620194 | 0.37620194 | 0.621071906 |
| Ni14 | 0.374760351 | 0.621610393 | 0.37650867 |
| Ni15 | 0.621610393 | 0.374760351 | 0.37650867 |
| Ni16 | 0.621597183 | 0.621597183 | 0.623712443 |
| Pr1 | 0.003658075 | 0.003658075 | 0.001278979 |
| Pr2 | 0.496341925 | 0.496341925 | 0.001278979 |
| Pr3 | 0.504115703 | 0.995884297 | 0.499873617 |
| Pr4 | 0.995884297 | 0.504115703 | 0.499873617 |
| (b) $Mg_3Pr_5Ni_{16}H_1$, $a$ = 7.21199472432647 Å | | | |
| atom | $x$ | $y$ | $z$ |
| H1 | 0.25 | 0.25 | 0.94965013 |
| Mg1 | 0.25 | 0.75 | 0.750127744 |
| Mg2 | 0.75 | 0.25 | 0.750127744 |
| Mg3 | 0.75 | 0.75 | 0.244443075 |
| Ni1 | 0.121788317 | 0.121788317 | 0.628407889 |
| Ni2 | 0.107488249 | 0.392511751 | 0.871566587 |
| Ni3 | 0.119591796 | 0.631282167 | 0.12577702 |
| Ni4 | 0.123125438 | 0.872578015 | 0.379991913 |
| Ni5 | 0.392511751 | 0.107488249 | 0.871566587 |
| Ni6 | 0.380408204 | 0.868717833 | 0.12577702 |
| Ni7 | 0.631282167 | 0.119591796 | 0.12577702 |
| Ni8 | 0.626582315 | 0.873417685 | 0.879582589 |
| Ni9 | 0.872578015 | 0.123125438 | 0.379991913 |

| (b) $Mg_3Pr_5Ni_{16}H_1$, $a$ = 7.21199472432647 Å | | | |
|---|---|---|---|
| atom | $x$ | $y$ | $z$ |
| Ni10 | 0.868717833 | 0.380408204 | 0.12577702 |
| Ni11 | 0.873417685 | 0.626582315 | 0.879582589 |
| Ni12 | 0.878613499 | 0.878613499 | 0.625156669 |
| Ni13 | 0.378211683 | 0.378211683 | 0.628407889 |
| Ni14 | 0.376874562 | 0.627421985 | 0.379991913 |
| Ni15 | 0.627421985 | 0.376874562 | 0.379991913 |
| Ni16 | 0.621386501 | 0.621386501 | 0.625156669 |
| Pr1 | 0.997923629 | 0.997923629 | 0.99590804 |
| Pr2 | 0.502076371 | 0.502076371 | 0.99590804 |
| Pr3 | 0.511741493 | 0.988258507 | 0.506307851 |
| Pr4 | 0.988258507 | 0.511741493 | 0.506307851 |
| Pr5 | 0.25 | 0.25 | 0.268716324 |
| (c) $Mg_5Pr_3Ni_{16}H_1$, $a$ = 7.0759387182277171 Å | | | |
| atom | $x$ | $y$ | $z$ |
| H1 | 0.255815732 | 0.255815732 | 0.988493192 |
| Mg1 | 0.003608807 | 0.003608807 | 0.000974263 |
| Mg2 | 0.238197777 | 0.238197777 | 0.262094777 |
| Mg3 | 0.236099203 | 0.761811668 | 0.762420398 |
| Mg4 | 0.761811668 | 0.236099203 | 0.762420398 |
| Mg5 | 0.764741888 | 0.764741888 | 0.231988316 |
| Ni1 | 0.120984904 | 0.120984904 | 0.627702883 |
| Ni2 | 0.109774584 | 0.37840756 | 0.876872144 |
| Ni3 | 0.117630285 | 0.635907226 | 0.121148097 |
| Ni4 | 0.122139843 | 0.880526819 | 0.368961147 |
| Ni5 | 0.37840756 | 0.109774584 | 0.876872144 |
| Ni6 | 0.373904593 | 0.874778289 | 0.122657947 |
| Ni7 | 0.635907226 | 0.117630285 | 0.121148097 |
| Ni8 | 0.632372061 | 0.877137829 | 0.877694484 |
| Ni9 | 0.880526819 | 0.122139843 | 0.368961147 |
| Ni10 | 0.874778289 | 0.373904593 | 0.122657947 |
| Ni11 | 0.877137829 | 0.632372061 | 0.877694484 |
| Ni12 | 0.880640078 | 0.880640078 | 0.630675148 |
| Ni13 | 0.374383254 | 0.374383254 | 0.62084556 |
| Ni14 | 0.372686417 | 0.621279985 | 0.37602487 |
| Ni15 | 0.621279985 | 0.372686417 | 0.37602487 |
| Ni16 | 0.621317509 | 0.621317509 | 0.624624095 |
| Pr1 | 0.497763205 | 0.497763205 | 0.00131883 |
| Pr2 | 0.503796373 | 0.99429411 | 0.49986238 |
| Pr3 | 0.99429411 | 0.503796373 | 0.49986238 |

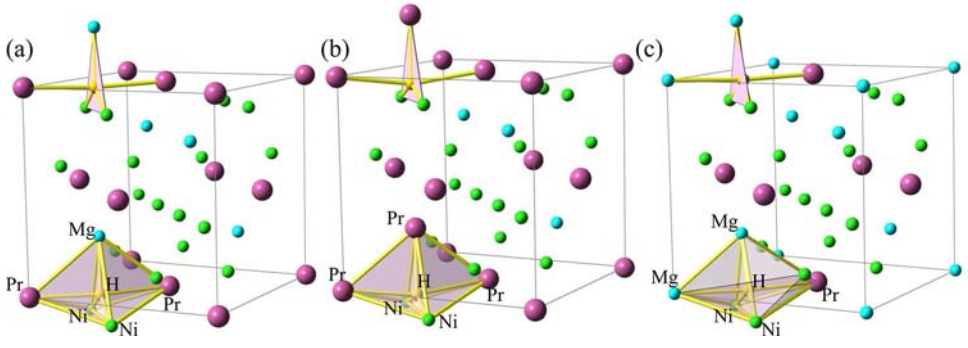


**Figure 5.** Shift of hydrogen occupation site by changing of the ratio of Mg/Pr using theoretical calculation; (a) $Mg_4Pr_4Ni_{16}H_1$, (b) $Mg_3Pr_5Ni_{16}H_1$, and (c) $Mg_5Pr_3Ni_{16}H_1$.

on the symmetry plane of the bipyramid, which is between two 48*h* sites (0.7363, 0.7363, 0.9979), because these sites are close. Figure 6 shows deuterium distributions in a C15b structure. The large yellow and red balls show deuterium atoms at 16*e* and 24*g* sites, respectively, which are separated by more than 2.1 Å in atomic distances from certain deuterium atoms at 16*e* sites.


dx.doi.org/10.1021/ic400528u | *Inorg. Chem.* 2013, 52, 7010−7019

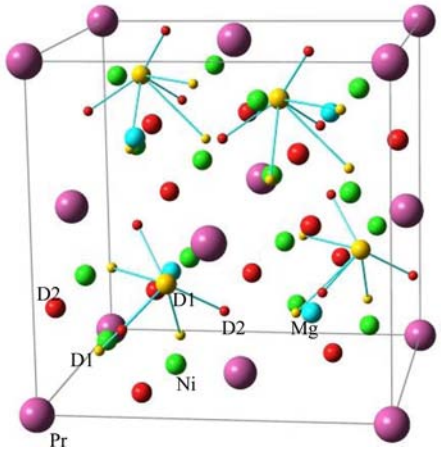


**Figure 6.** Atomic coordination of $Mg_{1.4}Pr_{0.6}Ni_4H_{\sim 3.6}$. Blue line indicates the shorter bond length between two deuterium atoms than 2.1 Å.

Small balls show deuterium atoms at 16*e* and 24*g* sites, respectively, which have a distance of less than 2.1 Å. There are four independent tetrahedrons built by deuterium at 16*e* sites in the unit cell. The distance of nearest-neighbor deuterium atoms at 16*e* sites is 2.06 Å, which is shown by the blue bar in Figure 6. This is slightly shorter than Westlake's empirical criteria.[39] Therefore, more than two deuterium atoms are unlikely to occupy the same tetrahedron simultaneously because of the repulsive D−D interaction. The maximum deuterium occupancy at a 16*e* site should be close to 0.25 from the viewpoint of geometry and Westlake's empirical criteria.[39] In fact, the refined deuterium occupancy was close to 0.25. Since the distance of the nearest neighboring deuterium at 24*g* site is 2.57 Å, the repulsive interactions are unlikely to play a role. However, the distance of the first and second nearest neighboring deuterium between the 16*e* and 24*g* sites is 1.50 Å and 2.75 Å, respectively, suggesting the nearest 24*g* sites to the occupied 16*e* site cannot be occupied. Taking the Westlake empirical criteria into consideration, if four deuterium atoms would occupy the 16*e* site, only half of the 24*g* site can be occupied by deuterium, suggesting that the occupancy is less than 0.5 at the 24*g* site. This means that the occupancy at the 48*h* site is less than 0.25. In fact, the refined value was 0.20. Therefore, our experimental results indicate that deuterium atoms are maximally occupied at both 16*e* and 24*g* sites in keeping with Westlake empirical criteria.

Here, we would like to discuss the difference between the average and local structures. As described above, $Mg_{1.4}Pr_{0.6}Ni_4D_{\sim 3.6}$ showed the C15b structure in average. To simplify the model, the deuterium occupation site is assumed to be the 24*g* site again. Figure 7a,b shows the atomic coordination for the average structure of $Mg_{1.4}Pr_{0.6}Ni_4H_{\sim 3.6}$. In these figures, deuterium atoms which were less than 2.1 Å in atomic distances from certain deuterium atoms at 16*e* sites were removed. One Pr atom has possible bonding with four deuterium atoms inside a $PrNi_3$ tetrahedron (16*e* site) and with 12 deuterium atoms inside a $Pr_2MgNi_2$ triangular bipyramid (24*g* site). Taking the occupancy from our present refinement and the Westlake empirical criteria into consideration, one Pr atom has interaction with one deuterium atom inside of the $PrNi_3$ tetrahedron and with six deuterium atoms inside the $Pr_2MgNi_2$ triangular bipyramid as shown in Figure 7a,b. On the other hand, $Mg_{1.4}Pr_{0.6}Ni_4D_{\sim 3.6}$ was locally distorted to make an orthorhombic hydride. In the orthorhombic structure, the deuterium atoms are located in two types of $Pr_2MgNi_2$ triangular bipyramid and $PrNi_3$ tetrahedron.[6,8] One Pr atom in the orthorhombic structure interacts with two deuterium atoms inside of the $Pr_2MgNi_2$ triangular bipyramid (2*a* site) and with four deuterium atoms inside different $Pr_2MgNi_2$ triangular bipyramid (4*b* site) and with one deuterium atom inside a $PrNi_3$ tetrahedron (2*a* site) as shown in Figure 7c,d. When Figure 7a and Figure 7c or Figure 7b and Figure 7d are compared, the coordination of deuterium atoms obtained from the average and local structures was consistent with each other, although the metal atoms slightly deviated. This also suggests that the larger atomic displacement parameters for metal atoms obtained via Rietveld refinement come from the deviation of the metal atoms.

**4.2. Local Distortion in $Mg_{1.4}Pr_{0.6}Ni_4D_{\sim 3.6}$.** Here we would like to discuss why the local distortion appears in $Mg_{1.4}Pr_{0.6}Ni_4D_{\sim 3.6}$. A well-known example of a compound exhibiting a difference between its average structure and local structure is $LaMnO_3$ at elevated temperature.[40] $LaMnO_3$ shows a phase transformation at around 750 K during heating from an orthorhombic structure with space group *Pbnm* to a cubic-like structure with space group *Pbnm*.[40,41] From the average structure model, $LaMnO_3$ has three different Mn−O bond lengths below 750 K and only one bond length above 750 K. However, PDF analysis clearly showed three different Mn−O

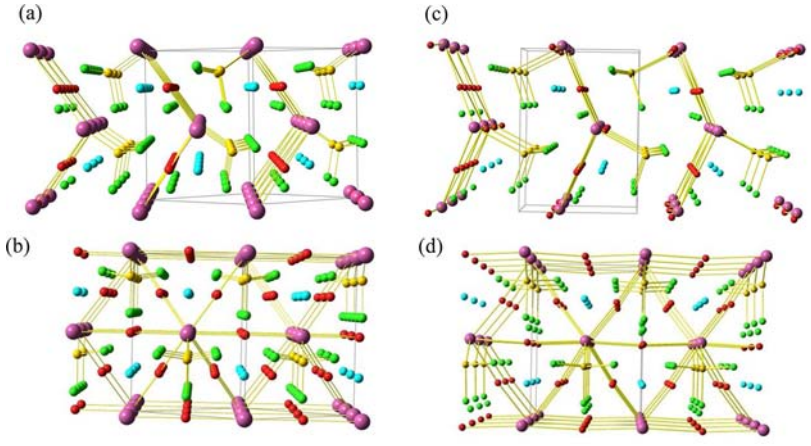


**Figure 7.** Comparison of atomic coordination between average and local structures of $Mg_{1.4}Pr_{0.6}Ni_4H_{\sim 3.6}$; (a) average structure from $(\bar{1}10)$, (b) average structure from (110), (c) local structure from (100), and (d) local structure from (010).


dx.doi.org/10.1021/ic400528u | *Inorg. Chem.* 2013, 52, 7010−7019

bond lengths locally in a cubic-like structure as well as the orthorhombic structure. This suggests that the structural characteristic (varying Mn−O bond lengths) in the low temperature phase remains in the local order at high temperature, where the average structure is different. Therefore, one possibility for the local distortion in $Mg_{1.4}Pr_{0.6}Ni_4D_{\sim 3.6}$ is that the orthorhombic structure would be more stable than the C15b structure at low temperature. If it is true, C15b $Mg_{1.4}Pr_{0.6}Ni_4D_{\sim 3.6}$ would transform to the orthorhombic structure below 100 K. This possibility is supported by the theoretical calculation for $Mg_{1.0}Ce_{1.0}Ni_4$ and $Mg_{1.0}Y_{1.0}Ni_4$ showing that the orthorhombic hydride is more stable than the C15b hydride.[12,42] At present, however, there is no experimental evidence for the phase transformation between the orthorhombic and the C15 structure. Another possibility comes from the composition of $Mg_{2-x}Pr_xNi_4$. The deuterium occupation sites were known to be $AB_3$ and $A_2B_2$ sites in C15 structure, while those were $PrNi_3$ and $Pr_2MgNi_2$ sites in $Mg_{1.0}Pr_{1.0}Ni_4D_{\sim 4}$ and those were $PrNi_3$ and $PrMgNi_2$ sites in $Mg_{1.4}Pr_{0.6}Ni_4D_{\sim 3.6}$. By Mg substitution into Pr, the deuterium atoms in $Pr_2MgNi_2$ shifted from on the symmetry plane of $MgNi_2$ to off the plane, e.g., toward the center of the $PrMgNi_2$ tetrahedron. If the amount of Mg substitution is small, only a small fraction of deuterium atoms would shift the symmetry plane. By increasing the fraction of Mg, the number of deuterium atoms which shift toward the center of the $PrMgNi_2$ tetrahedron would increase. Consequently, a cubic structure would be stabilized in Mg-rich $Mg_{2-x}Pr_xNi_4$ with an increase of Mg content, as seen in hydrides with a C15 structure, while an orthorhombic structure should remain in the local order with a decrease of Mg content. Therefore, our present data suggest that such a local distortion should not be observed in more Mg-rich $Mg_{2-x}Pr_xNi_4$. In contrast, $Mg_{2-x}Pr_xNi_4$ with $0.6 < x < 1.0$ should show the local orthorhombic distortion until a higher $r$ region.

## 5. CONCLUSIONS

We investigated the crystal structure and the local structure of $Mg_{2-x}Pr_xNi_4$ deuterides using neutron total scattering and first-principles calculations to understand the origins of different crystal structures of these deuterides and to observe the local distortion upon deuterium absorption.

Our results highlight several interesting features of these compounds. The crystal structure and the deuterium occupation sites changed with the Mg/Pr ratio in $Mg_{2-x}Pr_xNi_4D_y$: $Mr_{1.0}Pr_{1.0}Ni_4$ forms the orthorhombic deuteride with three occupation sites (two types of $Pr_2MgNi_2$ triangular bipyramid and $PrNi_3$ tetrahedron), and $Mg_{1.4}Pr_{0.6}Ni_4$ forms the C15b deuteride with two occupation sites ($PrNi_3$ tetrahedron and $PrMgNi_2$ tetrahedron). The preferential crystal structure and deuterium occupation sites were determined by whether the $Pr_2MgNi_2$ triangular bipyramid is symmetric or asymmetric to the $MgNi_2$ plane depending on the Mg/Pr ratio. The asymmetric shape of the triangular bipyramid, for Mg-rich compounds results in the deuterium shifting off the Mg-Ni-Ni symmetry plane and serves to stabilize the cubic C15b structure on average. However, the orthorhombic structure survives locally in $Mg_{1.4}Pr_{0.6}Ni_4D_{\sim 3.6}$.

## AUTHOR INFORMATION

### Corresponding Author

*E-mail: kouji.sakaki@aist.go.jp.

### Notes

The authors declare no competing financial interest.

## ACKNOWLEDGMENTS

Part of this work was supported by New Energy and Industrial Technology Development Organization (NEDO) under its "Advanced Fundamental Research Project on Hydrogen Storage Materials" and "Development of technologies for hydrogen production, delivery and storage system". We thank Joan Siewenie for help with the experiments. Work performed at the Lujan Neutron Scattering Center was funded by the DOE Office of Basic Energy Sciences. Los Alamos National Laboratory is operated by Los Alamos National Security LLC under Contract DE-AC52-06NA25396.

## REFERENCES

(1) Kadir, K.; Sakai, T.; Uehara, I. *J. Alloys Compd.* **1997**, *257*, 115−121.
(2) Kadir, K.; Kuriyama, N.; Sakai, T.; Uehara, I.; Eriksson, L. *J. Alloys Compd.* **1999**, *284*, 145−154.
(3) Kadir, K.; Sakai, T.; Uehara, I. *J. Alloys Compd.* **1999**, *287*, 264−270.
(4) Kohno, T.; Yoshida, H.; Kawashima, F.; Inaba, T.; Sakai, I.; Yamamoto, M.; Kanda, M. *J. Alloys Compd.* **2000**, *311*, L5−L7.
(5) Aono, K.; Orimo, S.; Fujii, H. *J. Alloys Compd.* **2000**, *309*, L1−L4.
(6) Chotard, J.-N.; Sheptyakov, D.; Yvon, K. *Z. Kristallogr.* **2008**, *223*, 690−696.
(7) Oesterreicher, H.; Bittner, H. *J. Less-Common Met.* **1980**, *73*, 339−344.
(8) Guenee, L.; Favre-Nicolin, V.; Yvon, K. *J. Alloys Compd.* **2003**, *348*, 129−137.
(9) Bobet, J.-L.; Lesportes, P.; Roquefere, J.-G.; Chevalier, B.; Asano, K.; Sakaki, K.; Akiba, E. *Int. J. Hydrogen Energy* **2007**, *32*, 2422−2428.
(10) Stan, C.; Andronescu, E.; Asano, K.; Sakaki, K.; Bobet, J.-L. *Int. J. Hydrogen Energy* **2008**, *33*, 2053−2058.
(11) Stan, C.; Asano, K.; Sakaki, K.; Akiba, E.; Couillaud, S.; Bobet, J.-L. *Int. J. Hydrogen Energy* **2009**, *34*, 3038−3043.
(12) Roquefere, J.-G.; Matar, S. F.; Huot, J.; Bobet, J.-L. *Solid State Science* **2009**, *11*, 1971−1978.
(13) Terashita, N.; Sakaki, K.; Tsunokake, S.; Nakamura, Y.; Akiba, E. *Mat. Trans.* **2012**, *53*, 513−517.
(14) Sakaki, K.; Terashita, N.; Tsunokake, S.; Nakamura, Y.; Akiba, E. *J. Phys. Chem. C* **2012**, *116*, 19156−19163.
(15) Sakaki, K.; Terashita, N.; Tsunokake, S.; Nakamura, Y.; Akiba, E. *J. Physical Chemistry C* **2012**, *116*, 1401−1407.
(16) Inui, H.; Yamamoto, T.; Hirota, M.; Yamaguchi, M. *J. Alloys. Compd.* **2002**, *320*−*332*, 117−124.
(17) Wu, E.; Kisi, E. H.; Gray, E.; Mac, A. *J. Appl. Crystallogr.* **1998**, *31*, 363−368.
(18) Cerny, R.; Joubert, J.-M.; Latroche, M.; Percheron-Guegan, A.; Yvon, K. *J. Appl. Crystallogr.* **2000**, *33*, 997−1005.
(19) Joubert, J.-M.; Latroche, M.; Cerny, R.; Percheron-Guegan, A.; Yvon, K. *J. Alloys Compd.* **2002**, *330*−*332*, 208−214.
(20) Kisi, E. H.; Wu, E.; Kemali, M. *J. Alloys Compd.* **2002**, *330*−*332*, 202−207.
(21) Nakamura, Y.; Akiba, E. *J. Alloys Compd.* **2000**, *308*, 309−318.
(22) Nakamura, Y.; Bowman, R. C.; Akiba, E. *J. Alloys Compd.* **2004**, *373*, 183−193.
(23) Decamps, B.; Joubert, J.-M.; Cerny, R.; Percheron-Guegan, A. *J. Alloys Compd.* **2005**, *404*−*406*, 570−575.
(24) Shirai, Y.; Araki, H.; Mori, T.; Nakamura, W.; Sakaki, K. *J. Alloys Compd.* **2001**, *330*−*332*, 125−131.
(25) Sakaki, K.; Akiba, E.; Mizuno, M.; Araki, H.; Shirai, Y. *J. Alloys Compd.* **2009**, *473*, 87−93.
(26) Sakaki, K.; Date, R.; Mizuno, M.; Araki, H.; Nakamura, Y.; Shirai, Y.; Bowman, R. C.; Akiba, E. *J. Alloys Compd.* **2009**, *477*, 205−211.
(27) Egami, T.; Billinge, S. J. L. *Underneath the Bragg Peaks: Structural Analysis of Complex Materials*; Pergamon Press Elsevier: Oxford, England, 2003.

(28) Proffen, T.; Egami, T.; Billinge, S. J. L.; Cheetham, A. K.; Louca, D.; Parise, J. B. *Appl. Phys. A: Mater. Sci. Process.* **2002**, *74*, S163−S165.
(29) Peterson, P. F.; Gutmann, M.; Proffen, Th.; Billinge, S. J. L. *J. Appl. Crystallogr.* **2000**, *33*, 1192.
(30) Farrow, C. L.; Juhas, P.; Liu, J. W.; Bryndin, D.; Božin, E. S.; Bloch, J.; Proffen, Th.; Billinge, S. J. L. *J. Phys.: Condens. Matter* **2007**, *19*, 335219.
(31) Proffen, T.; Billinge, S. J. L.; Egami, T.; Louca, D. *Z. Kristallogr.* **2003**, *218*, 132−143.
(32) Larson, A. C.; Von Dreele, R. B. General Structure Analysis System (GSAS); Los Alamos National Laboratory Report No. LAUR 86-748; Los Alamos National Laboratory: Los Alamos, NM, 2004.
(33) Toby, B. H. *J. Appl. Crystallogr.* **2001**, *34*, 210−213.
(34) Kresse, G.; Furthmuller, J. *Comput. Mater. Sci.* **1996**, *6*, 15−50.
(35) Kresse, G.; Furthmuller, J. *Phys. Rev. B* **1996**, *54*, 11169−11186.
(36) Perdew, J. P.; Burke, K.; Ernzerhof, M. *Phys. Rev. Lett.* **1996**, *77*, 3865−3868.
(37) Kresse, G.; Joubert, D. *Phys Rev. B* **1999**, *59*, 1758−1775.
(38) Blöchl, P. E. *Phys. Rev. B* **1994**, *50*, 17953−17979.
(39) Westlake, D. G. *J. Less-Common Met.* **1983**, *91*, 1−20.
(40) Qiu, X.; Proffen, T.; Mitchell, J. F.; Billinge, S. J. L. *Phys. Rev. Let.* **2005**, *94*, 177203.
(41) Rodriguez-Carvajal, J.; Hennion, M.; Moussa, F.; Moudden, A. H. *Phys. Rev. B* **1998**, *57*, 3189−3192.
(42) Prigent, J.; Gupta, M. *J. Alloys Compd.* **2007**, *446*−*447*, 90−95.